

**Effective diffusivity of cement pastes from virtual microstructures  
Role of gel porosity and capillary pore percolation**

Patel, Ravi A.; Perko, Janez; Jacques, Diederik; De Schutter, Geert; Ye, Guang; van Breugel, K.

**DOI**

[10.1016/j.conbuildmat.2018.01.010](https://doi.org/10.1016/j.conbuildmat.2018.01.010)

**Publication date**

2018

**Document Version**

Final published version

**Published in**

Construction and Building Materials

**Citation (APA)**

Patel, R. A., Perko, J., Jacques, D., De Schutter, G., Ye, G., & van Breugel, K. (2018). Effective diffusivity of cement pastes from virtual microstructures: Role of gel porosity and capillary pore percolation. *Construction and Building Materials*, 165, 833-845. <https://doi.org/10.1016/j.conbuildmat.2018.01.010>

**Important note**

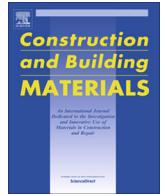
To cite this publication, please use the final published version (if applicable).  
Please check the document version above.

**Copyright**

Other than for strictly personal use, it is not permitted to download, forward or distribute the text or part of it, without the consent of the author(s) and/or copyright holder(s), unless the work is under an open content license such as Creative Commons.

**Takedown policy**

Please contact us and provide details if you believe this document breaches copyrights.  
We will remove access to the work immediately and investigate your claim.



# Effective diffusivity of cement pastes from virtual microstructures: Role of gel porosity and capillary pore percolation

Ravi A. Patel<sup>a,b,\*</sup>, Janez Perko<sup>a</sup>, Diederik Jacques<sup>a</sup>, Geert De Schutter<sup>b</sup>, Guang Ye<sup>b,c</sup>, Klaas Van Bruegel<sup>c</sup>

<sup>a</sup> Institute for Environment, Health, and Safety (EHS), Belgian Nuclear Research Centre (SCK•CEN), Boeretang 200, B2400 Mol, Belgium

<sup>b</sup> Magnel Laboratory for Concrete Research, Department of Structural Engineering, Ghent University, B9052 Ghent, Belgium

<sup>c</sup> Microlab, Faculty of Civil Engineering and Geosciences, Delft University of Technology, P.O. 9 Box 5048, 2600 GA Delft, The Netherlands

## HIGHLIGHTS

- The percolation threshold at around 20% of capillary porosity required for correct predictions.
- Differences between diffusivity obtained from different techniques due to difference in contribution of gel pores.
- Constrictivity parameter for C-S-H is 1/10.

## ARTICLE INFO

### Article history:

Received 4 May 2017

Received in revised form 20 November 2017

Accepted 2 January 2018

Available online 20 February 2018

### Keywords:

Microstructure modelling

Diffusivity

Transport properties

Cement paste

## ABSTRACT

The role of capillary pores percolation and gel pores are investigated to explain the underlying differences between relative diffusivity obtained from different experimental techniques using microstructures generated from two different types of hydration model viz., CEMHYD3D (a voxel based approach) and HYMOSTRUC (a vector based approach). These models provide microstructures with different capillary pore connectivity for the same degree of hydration and the same porosity due to the underlying assumptions. In order to account for a C-S-H diffusivity at the micro-scale, a continuum micro-mechanics based model has been proposed. These simulations show that depercolation of capillary pores at around 20% of capillary porosity is essential in order to correctly predict diffusivity of cement paste with water-cement ratio by mass (w/c) in between 0.4 and 0.5. Furthermore from our analysis we present a viable postulate that the higher diffusivity measured by electric resistivity compared to other methods is due to differences in contribution from gel pores. For electrical resistivity measurement it is proposed that all gel pores are diffusive whereas for ion and tracer transport it is proposed that only nitrogen accessible gel pores are diffusive.

© 2018 Elsevier Ltd. All rights reserved.

## 1. Introduction

Diffusivity is a crucial parameter to assess the impact of several deterioration mechanisms such as sulphate attack, leaching, carbonation, chloride transport for coastal concrete structures, and to predict contaminant transport in cementitious barriers in hazardous waste disposal systems. It is also used as a key durability indicator to define the service life of concrete structures. Diffusivity is closely related to the morphological features of concrete which exhibits a complex multi-scale nature [1]. Morphological hetero-

geneities of concrete from modeling point of view can be conceptually divided into different material scales as shown in Fig. 1 viz., macro-, meso-, micro-, sub-micro- and nano-scales [1]. At the macro-scale cementitious material is treated as continuum; at meso-scale, aggregates, interface transition zone (ITZ) and cement paste are explicitly represented; at micro-scale heterogeneities at the cement paste are represented however C-S-H phase is treated as a continuum; heterogeneities in the C-S-H phase are resolved at sub-micro- and nano-scales. It has been shown by recent compilation of experimental data on mortar and concrete diffusivity by Patel et al. [2] and through numerical modeling by Bentz et al. [3], that the contribution of ITZ to diffusivity is negligible. Consequently, diffusivity can be described solely in terms of the volume fractions of aggregates and cement paste. Patel et al. [2] also reported that different experimental techniques result in differences in the values of relative diffusivity of cementitious

\* Corresponding author at: Institute for Environment, Health, and Safety (EHS), Belgian Nuclear Research Centre (SCK•CEN), Boeretang 200, B2400 Mol, Belgium.

E-mail addresses: [rpatel@sckcen.be](mailto:rpatel@sckcen.be) (R.A. Patel), [jperko@sckcen.be](mailto:jperko@sckcen.be) (J. Perko), [djacques@sckcen.be](mailto:djacques@sckcen.be) (D. Jacques), [Geert.DeSchutter@ugent.be](mailto:Geert.DeSchutter@ugent.be) (G. De Schutter), [G.Ye@tudelft.nl](mailto:G.Ye@tudelft.nl) (G. Ye), [K.VanBruegel@tudelft.nl](mailto:K.VanBruegel@tudelft.nl) (K. Van Bruegel).

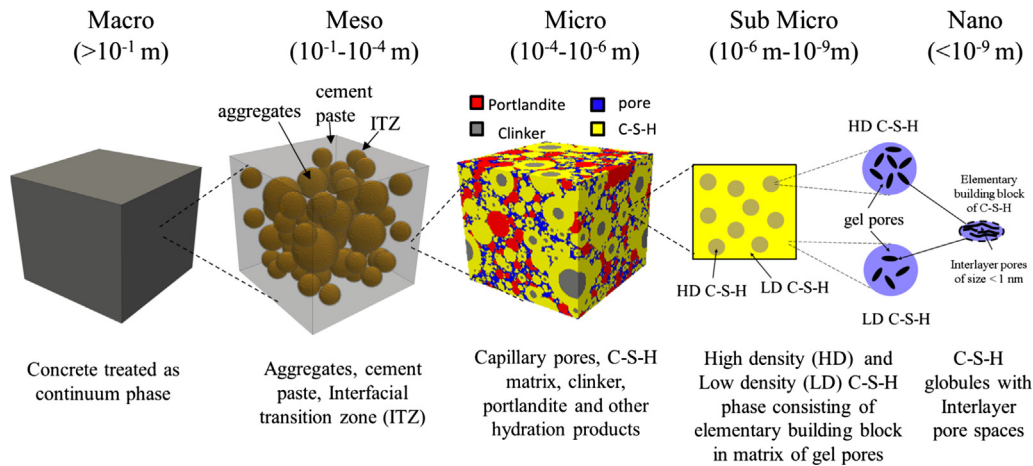


Fig. 1. Multi-scale representation of morphological heterogeneities of concrete from modeller's view point.

materials (relative diffusivity is the ratio of effective diffusivity of a porous medium to that of the tracer in water). Especially, diffusivities obtained from electric resistivity experiments are higher compared to those from other techniques. Differences are more prominent at lower water-cement ratio ( $w/c$ ) and mainly manifests at the micro- and lower scales which cannot be explained using existing analytical models based on effective media theory. As, at these scales diffusion occurs mainly through gel and capillary pores, one needs to understand and differentiate the influence of gel pores and capillary pores connectivity on diffusivity to explain the discrepancies between different experimental results.

In this study, cement paste morphology is generated using three dimensional hydration models to better understand the role of gel pores and capillary pores connectivity on diffusivity. These hydration models can be classified as suggested by Thomas et al. [4] based on the conceptual assumptions used for representing the cement particles into vector based models (e.g. HYMOSTRUC [5–8] and  $\mu ic$  [9]) and voxel based models (e.g. CEMHYD3D [10,11] and HydratiCA [12]). These hydration models have been calibrated to obtain the evolution of the microstructure and morphology taking into account the reactions at the cement particle level as a starting point, and considering the effects of particle size distribution, chemical composition of cement paste, water-cement ratio by mass ( $w/c$ ) and curing on hydration. However, the simulated cement paste morphology differ substantially between different hydration models for the same volume fraction of hydration products and capillary porosity. For example, the capillary pore depreculation occurs at around 5% [13] and 18 to 20% [14,15] for HYMOSTRUC and CEMHYD3D generated microstructures, respectively (irrespective of  $w/c$  ratio) for 1  $\mu m$  resolution. Thus, for the same capillary porosity one can achieve different connectivity from these models. Therefore in this study utilizing both CEMHYD3D (available in VCCTL software [16]) and HYMOSTRUC (modified version which includes nucleation and growth of portlandite [8]) allows us to investigate the role of capillary pore percolation.

At the micro-scale, the C-S-H phase containing sub-micro- and nano-scale porosity, i.e., gel porosity is treated as a continuum media due to the limitation of resolution within the simulation. However, diffusivity of the C-S-H phase is very difficult to measure and is often fitted by calibration of models using experimental data of cement paste. For virtual microstructures generated from CEMHYD3D, Garboczi and Bentz [17] suggested value 0.0025 for the relative diffusivity of C-S-H based on the calibration using steady state chloride ion diffusion experiments of [18,19]. These experiments were carried out for  $w/c$  ratios in the range of 0.3–0.7. Bentz et al. [20] using this value for C-S-H diffusivity and CEMHYD3D generated microstructures showed that good predictions (within

factor 2 bounds) can be achieved for cement paste diffusivity even for the low  $w/c$  ratio. Bentz et al. [21] using overlapping sphere models from C-S-H and assuming that the transport occurs only through cluster level pores computed relative diffusivity of 0.0033. Kamali-Bernard et al. [22] obtained a value of 0.001 for the relative diffusivity of C-S-H by fitting diffusivity obtained using CEMHYD3D microstructures to the experimental data of [23] at a  $w/c$  ratio of 0.25. Ma et al. [24] proposed the value of 0.00775 for the relative diffusivity of the C-S-H phase based on electric conductivity measurements using the diffusion model of Oh and Jang [25]. Recently, Ma et al. [26] developed a two-scale approach to determine the diffusivity of cement paste from virtual microstructures. The microstructure of cement paste is generated using a vector based approach analogous to HYMOSTRUC. The diffusivity of C-S-H phase was determined considering that transport occurs only through low density (LD) C-S-H which is simulated using a modified hard-cores/soft shell model. On comparison with the experimental data for electric resistivity they observed that their predictions do not comply well at later stage of hydration and for low  $w/c$ . Thus there is no general consensus on a unilateral value of C-S-H diffusivity. Therefore in this study, a continuum micro-mechanics based model to predict diffusivity of C-S-H phase has been proposed which predicts diffusivity of C-S-H considering its morphological features. Finally, diffusivity of cement paste is estimated from virtual microstructure using lattice Boltzmann method wherein C-S-H phase is treated as a continuum phase with diffusivity value assigned using the proposed C-S-H diffusion model. Predictions are compared to data obtained from different experimental techniques to understand the role of gel pores and capillary pore connectivity on diffusivity of cement paste. The remainder of the paper is organized as follow. Section 2 presents the modelling approach wherein the governing equations for the computational homogenization approach to obtain the diffusivity from virtual microstructures are first presented. Following that a C-S-H diffusivity model is introduced. Section 3 compares experimental results and model predictions and discusses the roles of gel and capillary porosity in different types of experiments. Finally, conclusions are presented in Section 4.

## 2. Determination of effective diffusion coefficient from virtual microstructures

### 2.1. Computational homogenization approach to determine diffusivity

At the scale of cement paste microstructures, the computational domain consists of capillary pores ( $\Omega_p$ ), porous C-S-H phase ( $\Omega_{CSH}$ )

and solid phases such as clinkers and other crystalline hydration products such as portlandite ( $\Omega_c$ ). The mass transport at this scale is assumed to be described by the diffusion equation in absence of electro-kinetic effects

$$\begin{aligned} \partial_t \phi(x)C(x) + \nabla \cdot \vec{J}(x) &= 0 \quad \forall x \in \Omega \\ \vec{J}(x) &= -D_e(x)\nabla C(x) \end{aligned} \quad (1)$$

$$\begin{aligned} \phi(x) &= \begin{cases} 1 & \forall x \in \Omega_p \\ \phi_{CSH} & \forall x \in \Omega_{CSH} \\ 0 & \forall x \in \Omega_s \end{cases} \\ D_e(x) &= \begin{cases} D_0 & \forall x \in \Omega_p \\ D_{CSH} & \forall x \in \Omega_{CSH} \\ 0 & \forall x \in \Omega_s \end{cases} \\ \Omega_{CSH} \cup \Omega_p \cup \Omega_s &= \Omega, \Omega_{CSH} \cap \Omega_p \cap \Omega_s = \emptyset \end{aligned} \quad (2)$$

where  $C$  is the concentration [ $N^1L^{-3}T^0$ ],  $\vec{J}$  is the flux vector [ $N^1L^{-1}T^{-1}$ ],  $D_e$  is the effective diffusivity [ $N^0L^2T^{-1}$ ] and  $\phi$  are the porosities at a point  $x$  in simulation domain ( $\Omega$ ).  $\phi_{CSH}$  is the porosity of the C-S-H volume element.  $D_0$  and  $D_{CSH}$  is the diffusivity in water [ $N^0L^2T^{-1}$ ] and effective diffusivity of C-S-H phase [ $N^0L^2T^{-1}$ ], respectively. In this study, we set  $D_0$  to  $1 \text{ m}^2/\text{s}$  as we are interested in relative diffusivity. The model to compute the effective C-S-H diffusivity ( $D_{CSH}$ ) is presented in Section 2.2. Along the boundary of the non-diffusive solid phase ( $\Gamma_s$ ), the following condition is applied

$$\vec{J}|_{\Gamma_s} = 0 \quad (3)$$

The representative element volume (REV) analysis carried out by different researchers suggests that a cubic microstructure with length  $100 \mu\text{m}$  is a reasonable size for obtaining diffusivity from the microstructures [27–29]. Our preliminary calculations also confirmed this and it was found that the standard deviation of diffusivity was less than 0.01% for different realizations of the microstructure. Therefore in order to compute the diffusion coefficient, cubic REV of length  $100 \mu\text{m}$  with resolution of  $1 \mu\text{m}$  were generated using the hydration models. At this resolution, it is assumed that capillary porosity is completely resolved.

In order to determine the diffusion coefficient along a specific axis, a constant gradient was imposed through a Dirichlet boundary at opposite ends and all other boundaries are treated as periodic:

$$\begin{aligned} \text{Dirichlet along axis of measurement : } C(x=0) &= 1 \\ \&C(x=100 \mu\text{m}) &= 0 \\ \text{Periodic on other directions : } C(x=0) &= C(x=100 \mu\text{m}) \\ \&\nabla C \cdot \hat{n}(x=0) &= -\nabla C \cdot \hat{n}(x=100 \mu\text{m}) \end{aligned} \quad (4)$$

By solving the boundary value problem proposed by Eqs. (1)–(4) for a steady state, a homogenized diffusivity ( $D_e^*$ ) along axis of measurement can be obtained from the volume averaged flux and concentration gradients as follows

$$D_e^* = -\frac{\langle \vec{J} \rangle}{\langle \nabla C \rangle} \quad (5)$$

The volume average quantity ( $\bullet$ ) is defined as

$$\langle \bullet \rangle = \frac{1}{|\Omega|} \int_{\Omega} \bullet \, \Omega$$

The two relaxation time lattice Boltzmann method has been utilized in this study to solve the proposed boundary value problem and is detailed in Appendix A. Calculations of  $D_e^*$  for the  $100 \mu\text{m}^3$  microstructures generated with HYMOSTRUC and CEMHYD3D in

this study showed that  $D_e^*$  in the three directions differ by less than 0.1% which indicates that the generated microstructures are isotropic. Hence, values of  $D_e^*$  in this study are the average of the  $D_e^*$  in the x-, y- and z-directions.

## 2.2. C-S-H diffusivity model based on continuum micro-mechanics

Continuum micro-mechanics provides a framework to obtain an analytical estimate of effective diffusivity by approximating the morphology as well-defined inclusions (such as spheres, cylinders, ellipsoids) distributed randomly throughout a matrix material [30]. The continuum micro-mechanics approaches do not account for effects associated with constrictivity. Constrictivity accounts for phenomena such as narrowing of pores restricting the diffusion of species through the pore, anion exclusion and influence of adsorbed layer on diffusion. However, there is lack of experimental data on constrictivity parameter. Therefore as proposed by Bary and co-authors [31,32] constrictivity factor ( $\delta_{CSH}$ ) is taken as 1/10, i.e., value of diffusivity in gel pores ( $D_{gp}$ ) one order lower than the one in capillary pores. This value of constrictivity parameter has been suggested by them based on comparison with experimental data. Bordallo et al. [33] based on quasielastic neutron scattering experiments also suggested that the water diffusion is one order lower in gel pores compare to capillary pores. Later in this work we also study the sensitivity of this constrictivity parameter with respect to relative diffusivity. In order to obtain the effective diffusivity the morphology of the C-S-H is considered at two levels as shown in Fig. 2, and diffusivity at each level is obtained using differential effective media theory (see Appendix B for discussion on the choice of approach).

At level-II two types of C-S-H exists, viz. low density C-S-H (LD C-S-H) and high density C-S-H (HD C-S-H) which are assumed to be formed of the same type of inclusions (“basic building blocks (BBB)”) in a matrix of gel pores but differ in packing density and in turn in porosity [34–38]. These BBB have an inter-layer porosity of about 18% [35]. The water in the inter-layer pores (<1 nm [36]) is structural water which is chemically bound to the C-S-H platelets and therefore is unlikely to contribute to diffusive transport. Hence, these BBB are considered as a non-diffusive phase. Different shapes have been proposed for the BBB of C-S-H such as spheres [34], bricks [36,39], disks [40], foils and needles [41]. In this study, the shape of BBB are considered as an oblate spheroid with aspect ratio of 0.12 as suggested in [42] which corresponds to the observations by Garrault et al. [39] in SEM images.

From the perspective of mass transport, the important distinction can be made between gel pores (>1 nm) as pores accessible by nitrogen and measurable during nitrogen adsorption measurements and ones which are inaccessible by nitrogen but accessible by water vapour during water vapour adsorption measurements. Both LD and HD C-S-H contain nitrogen inaccessible pores. However, LD C-S-H additionally contains the nitrogen accessible pores which lowers the density of LD C-S-H [43,37].

The diffusion coefficient of both HD and LD C-S-H (at level-II) are obtained using the differential effective media theory which is given as [44]

$$\begin{aligned} D_i &= D_{gp}(\phi_i)^{1/(Y-X-Z)} \quad i \in \{LD - CSH, HD - CSH\} \\ X &= 3 \frac{R - R^2}{1 + 3R}, \quad Y = 3 \frac{9R^2 - 2R + 1}{(1 + 3R)^2}, \\ Z &= 3 \frac{4 - 24R + 36R^2 + 3R^3 - 9R^4}{(5 - 3R)(1 + 3R)^2} \end{aligned} \quad (6)$$

where  $\phi_{HD-CSH}$  and  $\phi_{LD-CSH}$  is the porosity of HD C-S-H and LD C-S-H, respectively.  $D_{HD-CSH}$ ,  $D_{LD-CSH}$  are the diffusion coefficient [ $L^2T^{-1}$ ] of

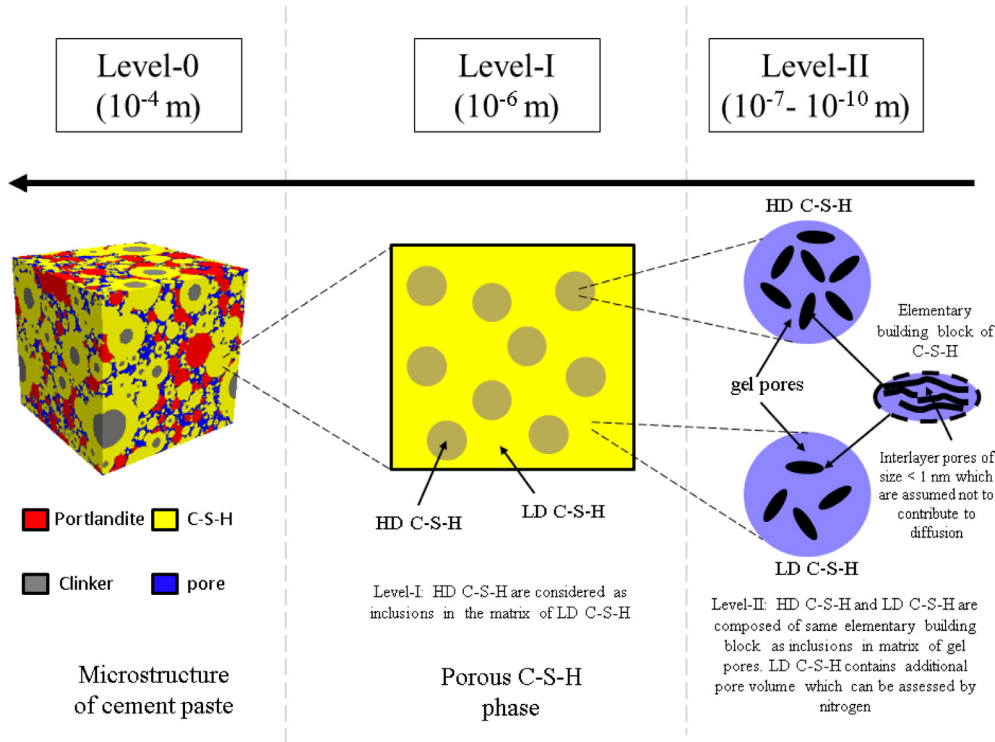


Fig. 2. A schematic representation of cement paste morphology.

HD C-S-H and LD C-S-H, respectively.  $R$  is the depolarization factor which is computed as

$$R = \frac{1 - \epsilon^2}{2\epsilon} \left( \ln \left( \frac{1 + \epsilon}{1 - \epsilon} \right) - 2\epsilon \right) \quad (\text{prolate spheroids})$$

$$R = \frac{1 + \epsilon^2}{\epsilon^3} (\epsilon - \tan^{-1} \epsilon) \quad (\text{oblate spheroids}) \quad (7)$$

$$\epsilon = \sqrt{1 - (a/c)^2}$$

where  $\epsilon$  is the eccentricity,  $a$  is the equatorial radius of the spheroid [L], and  $c$  is the distance from centre to pole along the symmetry axis [L]. The ratio of  $c$  to  $a$  is the aspect ratio. For oblate spheroids, the aspect ratio is less than one and thus provides a good representation for platelet like inclusions. Aspect ratio for prolate spheroids is greater than one and can be used to represent fibrous inclusions. For the asymptotic limits of aspect ratios, Eq. (6) reduces to

$$D_i = D_{gp}(\phi_i)^{5/3} \quad (\text{fibres})$$

$$D_i = D_{gp}(\phi_i)^{16/9} \quad (\text{disks}) \quad i \in \{LD - CSH, HD - CSH\} \quad (8)$$

At the scale of the smallest volume resolved in the microstructure model, i.e. level-I ( $1 \mu\text{m}^3$  volume element), representation of different types of C-S-H can be either made explicitly based on confinement conditions as proposed by Smilauer and Bittnar [45] or as a mixture of LD C-S-H and HD C-S-H. Smilauer and Bittnar [45] noted that the volume fraction obtained by their approach differed substantially from the model proposed by Tennis and Jennings [37] which is based on phenomenological considerations. Therefore, in this study C-S-H is represented as a mixture of LD and HD C-S-H with HD C-S-H assumed to consist of spherical inclusions in LD C-S-H as shown in Fig. 2. The volume fraction of LD and HD C-S-H are then determined using the model of [37]. The diffusivity of C-S-H volume element at level-I, can be determined using the differential effective media theory as follows [30,44]

$$\left( \frac{D_{HD-CSH} - D_{CSH}}{D_{HD-CSH} - D_{LD-CSH}} \right) \left( \frac{D_{LD-CSH}}{D_{CSH}} \right)^{1/3} = 1 - V_{HD-CSH} \quad (9)$$

where  $D_{CSH}$  is the effective diffusion coefficient of C-S-H [ $\text{L}^2\text{T}^{-1}$ ].  $V_{HD-CSH}$  is the volume fraction of HD C-S-H in the C-S-H.

For illustration of the proposed model,  $\phi_{HD-CSH}$  and  $\phi_{LD-CSH}$  are taken as 0.24 and as 0.37, respectively when all pores contribute [35] and 0 and 0.17, respectively when only nitrogen accessible pores contribute to diffusion [37]. A more detailed approach to compute  $V_{HD-CSH}$ ,  $\phi_{HD-CSH}$  and  $\phi_{LD-CSH}$ , which are the only parameters needed for the proposed model, based on model of Tennis and Jennings [37] is given in Appendix C. The relative diffusion coefficient obtained in the case when only nitrogen accessible pores are diffusive and when all gel pores are diffusive for different values of  $V_{HD-CSH}$  is shown in Fig. 3(a) and (b), respectively. Clearly, the case when all pores contribute to diffusion results in higher values of C-S-H diffusivity. At low w/c ratio, i.e. at high fraction of HD C-S-H, differences in C-S-H diffusivity can be up to an order of magnitude in two cases which can explain the higher diffusivity measured by electric resistivity techniques compared to other techniques at low w/c. Later on by comparison with experiments we show that the assumption that in the case of dissolved species and tracers only nitrogen accessible pore contribute, whereas, in electric resistivity measurement all pores contribute holds.

The proposed model also explains the differences in the values of C-S-H diffusivity obtained by different researchers. Garboczi and Bentz [17] proposed the value of relative C-S-H diffusivity as 0.0025 based on chloride diffusion (w/c in range of 0.3–0.7). Bentz et al. [20] using this value for C-S-H diffusivity and CEMHYD3D generated microstructures showed that good predictions (within factor 2 bounds) can be achieved for cement paste diffusivity even for the low w/c ratio. On the other hand, based on comparison with the tritiated water (HTO) diffusion at w/c equal to 0.25 Kamali-Bernard et al. [22] proposed a value of C-S-H diffusivity as 0.001. This differences in values of C-S-H proposed by different

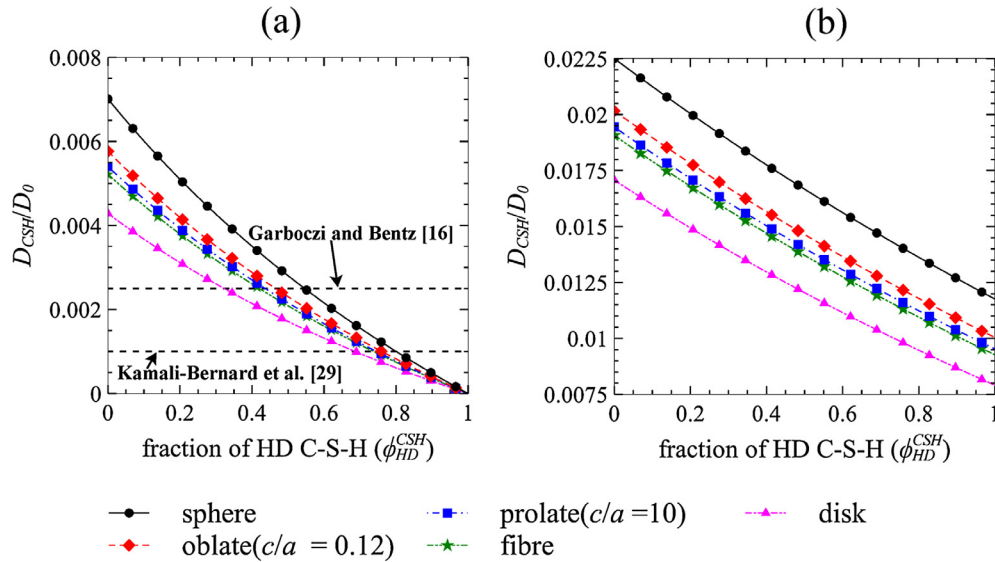


**Fig. 3.** Diffusion coefficient for C-S-H volume as predicted by proposed model (a) Only nitrogen accessible pore contributes to diffusion coefficient (b) all pores contribute to diffusion coefficient.

researchers can be explained in the present model by the difference in fraction of HD C-S-H at different w/c. Ma et al. [24] proposed C-S-H diffusivity in context of cement paste volume based on electric resistivity measurement as 0.0075. This value thus scale diffusivity with the volume fraction of C-S-H in cement paste and hence would be lower than that of the diffusivity of C-S-H. The value of the diffusivity of C-S-H volume element would fall in the range predicted by the proposed model taking into account the contribution of all pores. Fig. 3 shows that the shape of BBB of C-S-H can influence the estimated diffusivity of C-S-H phase and therefore a parametric study has been carried out later to access the influence of shape of BBB on diffusivity of cement paste.

Finally, to complete discussion on the proposed C-S-H model, assumptions made are summarized below –.

- The diffusion coefficients at each level can be homogenized using the differential effective media theory.
- The BBB for C-S-H is considered to be an oblate sphere with an aspect ratio of 0.12 for all simulations unless specified differently.
- The constrictivity factor for C-S-H diffusivity is considered as 1/10 unless specified differently.
- Diffusion of tracers and dissolved gases only occurs through the nitrogen accessible pores, whereas for electric resistivity all the gel pores contribute.

### 3. Result and discussions

#### 3.1. Experimental data used for comparison

We use a subset of the dataset collected by Patel et al. [2] to compare the diffusivity obtained from virtual microstructures generated using HYMOSTRUC and CEMHYD3D. It includes diffusivity obtained using different experimental techniques viz., electric-resistivity [24]; through-diffusion experiments with different tracers viz., HTO [47,48,23], dissolved gases such as helium [46] and oxygen [49]; and steady state chloride migration tests [50]. The cement composition and the curing conditions for the dataset is summarized in Tables 1 and 2, respectively. The dataset spans across a wide range of values for w/c and capillary porosity.

For datasets in which capillary porosity (porosity measured using MIP) was not available (data of [48,49,24]), Power's model was used to determine the capillary porosity, which is given as follows [51]

$$\phi_{cp} = \frac{w/c - 0.36\alpha}{w/c + 0.32} \quad (10)$$

where  $\alpha$  is the degree of hydration. For datasets, where the degree of hydration was not available (data of [48,49]), it was assumed that the paste has been hydrated to the maximum achievable degree of hydration, which is a reasonable assumption as the samples used in those experiments were well cured (summarized in Table 2). The maximum degree of hydration ( $\alpha_{max}$ ) was computed using relationship given in [48].

$$\alpha_{max} = 0.239 + 0.745 \tanh[3.62(w/c - 0.095)] \quad (11)$$

Fig. 4(a) shows the data which is used in this study to compare with numerical model. The experimental data on relative diffusivity obtained from the through-diffusion experiments and steady state chloride-migration experiments have values in same range. However, the values obtained from electric-resistivity are always higher compared to other techniques especially at a capillary porosity  $\leq 30\%$ . Fig. 4(b) shows values of relative diffusivity obtained from electrical-resistivity for the complete dataset collected in Patel et al. [2] from Refs. [52–54,24]. It can be noted that Ma et al. [24] chosen in this study closely corresponds to other datasets. The choice of Ma et al. [24] dataset was based on the fact that it covers wide range of w/c ratios with measurements reported at different cement hydration stages.

#### 3.2. Comparison of model predictions with experimental data

For comparison, virtual microstructures were generated from HYMOSTRUC and CEMHYD3D models using Bogue's composition and Blaine's fineness (summarized in Table 1) for w/c equal to those used in the experiments. Rosin-Ramler distribution is used for cement particle size distribution with parameters obtained from Blaine's fineness as discussed in [55]. Additional parameters required for both models were set to the default values of the models which has been well calibrated for OPC. Hydration was carried out till the required degree of hydration was achieved. The

**Table 1**  
Cement composition of the collected data.

Reference	Bouge composition (in %)				Fineness (m <sup>2</sup> /kg)
	C <sub>3</sub> S	C <sub>2</sub> S	C <sub>3</sub> A	C <sub>4</sub> AF	
Phung et al. [46]	66.06	15.21	8.9	9.83	435
Ma et al. [24]	65.37	15.10	10.35	9.17	-
Yamaguchi et al. [47]	54.77	24.38	12.26	8.59	-
Béjaoui and Bary [48]	67.08	17.88	3.79	6.09	310.5
Delagrave et al. [23] (w/c = 0.45)	68.99	6.56	7.87	4.44	461.6
Delagrave et al. [23] (w/c = 0.25)	69.04	7.14	8.16	4.68	535.1
Ngala and Page [49]	54.02	26.83	11.5	7.65	345
Sun et al. [50]	55.05	27.13	8.08	9.73	-

**Table 2**  
Curing conditions for the collected data.

Curing conditions	Reference
For 28 days in sealed condition in a controlled temperature of 22 °C ± 2 °C	Phung [46]
The samples were cured at 50 °C under deionized water until peak of in XRD of unhydrated cement phase disappears	Yamaguchi et al. [47]
Samples are cured in saturated lime water incorporating sodium and potassium hydroxide during 12 months	Béjaoui and Bary [48]
The specimens were demolded and immersed in lime solution for 3 months	Delagrave et al. [23]
After Curing at 22 °C for 2 weeks and immersed in 35 mM NaOH solution. They were then stored in a curing room at temperature of 38 ± 2 °C for 10 weeks	Ngala and Page [49]
The samples were placed in a room at a temperature of 20 °C for 24 h and then moved to a standard curing room (temperature of 20 ± 3 °C, relative humidity above 95%). After three days of curing, the samples were removed and split into several parts. Finally, the samples were taken out for measurement of their degree of hydration and porosity at the required standard age	Sun et al. [50]

capillary porosity for the generated microstructures was close to the experimental data for both models. However, pore connectivity differs substantially for generated microstructures from both models. Fig. 5 shows the fraction of capillary pore connected for cement composition of [48] for different w/c. Clearly, for HYMOSTRUC the capillary pore space remains the dominant phase for mass transport even at low w/c and low capillary porosities, whereas for

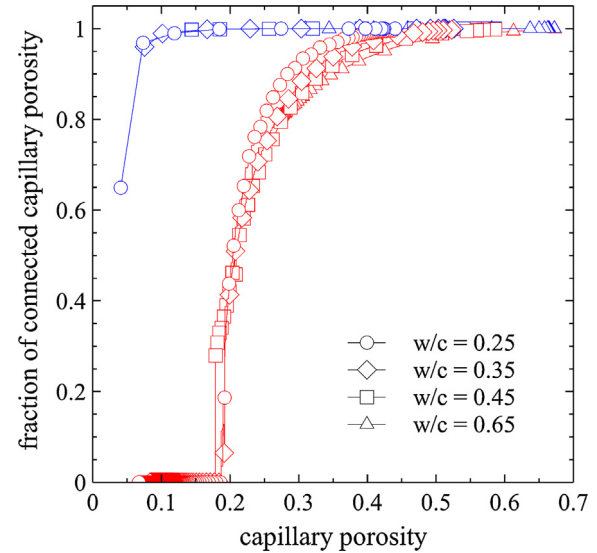


**Fig. 5.** Fraction of capillary pores percolated at different w/c during hydration for cement composition of Béjaoui and Bary [48]. The results for HYMOSTRUC and CEMHYD3D are marked blue and red respectively. (For interpretation of the references to colour in this figure caption, the reader is referred to the web version of this article.)

CEMHYD3D, at capillary porosities below 20%, the C-S-H phase and capillary pores connected through C-S-H phase would be the major phases for mass transport.

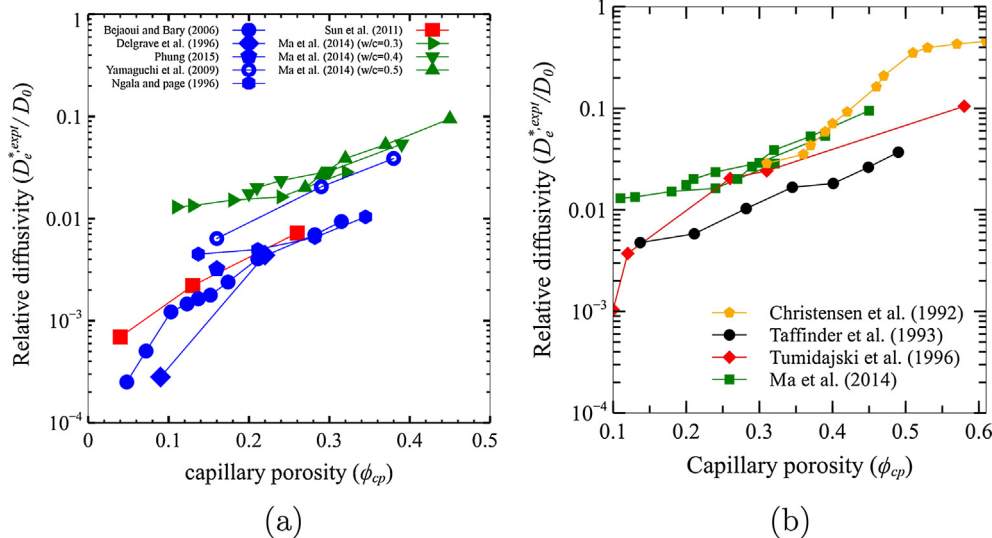


**Fig. 4.** Relative diffusivity with respect to capillary porosity (a) for all the collected experimental data used for comparison with numerical model (b) Data from different researchers for electrical resistivity as collected in Patel et al. [2].

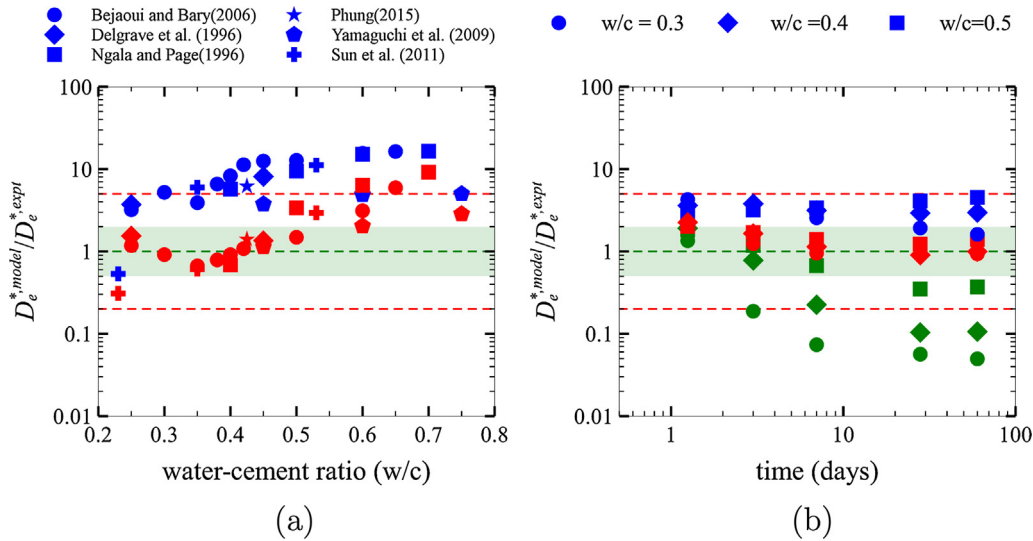


**Fig. 6.** Ratio between effective diffusivity predicted from virtual microstructure ( $D_e^{*model}$ ) and experimental data ( $D_e^{*expt}$ ) (a) with respect to w/c for through-diffusion and steady state electro-migration measurements, and (b) with respect to time in days for electric-resistivity measurements. Same marker type corresponds to same experimental dataset. Blue and red markers represents results from microstructures generated with HYMOSTRUC and CEMHYD3D, respectively. Green coloured markers in (b) represents results from microstructures generated from CEMHYD3D considering diffusion only through nitrogen accessible pores. The green area represents factor 2-bounds and dashed line in red shows factor 5-bounds. (For interpretation of the references to colour in this figure caption, the reader is referred to the web version of this article.)

### 3.2.1. Comparison with through-diffusion and steady state electro-migration experiments

Fig. 6(a) shows the ratio between effective diffusivity predicted from the virtual microstructure ( $D_e^{*model}$ ) and experimental data ( $D_e^{*expt}$ ) with respect to w/c for through-diffusion and steady state electro-migration tests. The effective diffusivity values obtained from microstructures generated with HYMOSTRUC are always higher than those using microstructures from CEMHYD3D which is line with the study of Liu et al. [56]. Zhang et al. [57] reduced the diffusivity in pore water (both capillary and C-S-H) by one order accounting for constrictivity effects in order to achieve good comparison between the experimental data and values obtained from microstructures generated from HYMOSTRUC. However, a more legible explanation for the over-estimations (about one-order of magnitude) obtained from the microstructures generated with HYMOSTRUC is due to the high degree of percolation of capillary pores at low w/c. From Fig. 5 it can be seen that even at 5% capillary porosity, 65% of the capillary pore space is connected. Fig. 7 shows the ratio of effective diffusivity computed from microstructures generated using CEMHYD3D and HYMOSTRUC. It can be clearly seen that the differences up to one order of magnitude exists at around 20% capillary porosity. This is the point when capillary pores reach complete depercolation for CEMHYD3D. The differences between diffusivity obtained from CEMHYD3D and HYMOSTRUC microstructures diminish beyond this point. This clearly illustrates that correct representation of capillary pore depercolation is necessary in the microstructure generated to ensure good predictions. Experimental study of San et al. [58] using measurements of chemical shrinkage, low temperature calorimetry, and electrical impedance spectroscopy also supports that the capillary porosity depercolation in cement pastes occurs at around 20%.

Variability in experimental values of diffusivity for through-diffusion and electro-migration is up to a factor 5-bounds with most values lie between a factor 2-bounds [2].<sup>1</sup> Therefore, predictions between factor 2-bounds serves as a good indicator to quantify

the predictability of models compared to experimental data. For HYMOSTRUC generated microstructures, all the predicted data points (except one) fall outside the factor 2-bounds and many of predictions fall outside factor 5-bounds. For CEMHYD3D generated microstructures, around 61% (of 23 simulated data points) lie within a factor 2-bounds and most of the predictions lie within a factor 5-bounds. This is comparable with the performance of existing analytical models as discussed in detail in [2].

### 3.2.2. Comparison with electric-resistivity data

For the case of electric-resistivity measurements, good predictions are observed under the assumption that all the gel pores contribute to the measurement as shown in Fig. 6(b). The assumption that only the nitrogen accessible pores in C-S-H contribute to diffusion which has been used to estimate diffusivity for through diffusion and steady state electro-migration experiments, give very low relative diffusion coefficients compared to experimental values. Therefore it can be deduced that the experimentally observed differences between electric-resistivity and through diffusion and electro-migration experiments manifests from the differences in the contribution from gel pores.

For the electric-resistivity measurements, differences between HYMOSTRUC and CEMHYD3D are lower compared to through-diffusion and electro-migration tests. This is due to a less pronounced difference between C-S-H diffusivity and diffusivity in capillary pore phase. The C-S-H diffusivity is relatively higher when all gel pores contribute to diffusivity which reduces the effect of capillary pore depercolation.

Variability in the experimental values obtained with electric resistivity measurements are within factor 5-bounds [2]. For CEMHYD3D generated microstructures, around 87% (of 15 simulated data points) of the predictions lie in factor 2-bounds and all predictions lie between factor of 5-bounds showing better performance compared to existing analytical models as discussed in Patel et al. [2]. For HYMOSTRUC generated microstructures, a large amount of the predictions lie beyond factor 2-bounds, although all of them fall within factor 5-bounds.

The electric-resistivity method is often used as a non-destructive, in situ technique to indirectly measure resistance of concrete against chloride ingress [59–61] and recently several

<sup>1</sup> The factor 5-bounds and factor 2-bounds refers to the area in between the line drawn by multiplying and dividing five and two, respectively with the line of equality).

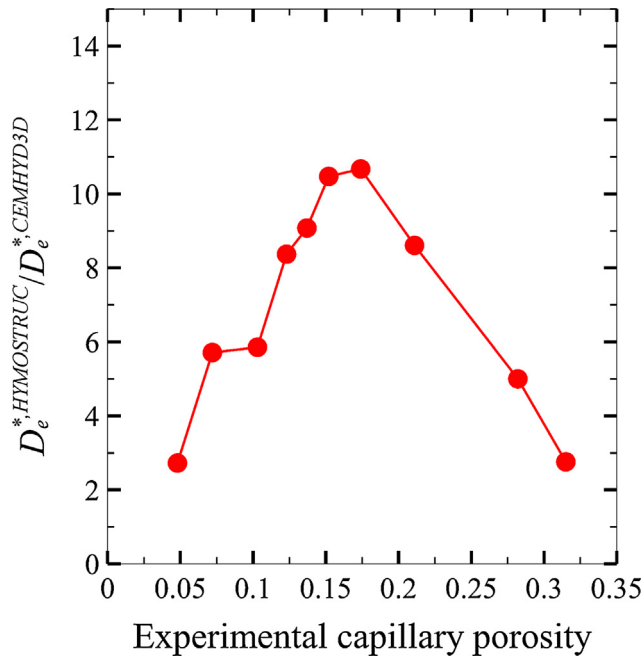


**Fig. 7.** Ratio of effective diffusivity predicted from virtual microstructures generated from HYMOSTRUC ( $D_e^{*HYMOSTRUC}$ ) and CEMHYD3D ( $D_e^{*CEMHYD3D}$ ) as a function of experimental capillary porosity for experimental data of Béjaoui and Bary [48].

researchers have tried to establish the relationship between electric resistivity and chloride diffusivity of concrete as [62–64]

$$D_e^{*,Cl} = k_{Cl} \frac{1}{\rho_e^*} \quad (12)$$

where  $\rho_e^*$  is the effective resistivity [ $ML^3T^{-3}Q^{-2}$ ],  $D_e^{*,Cl}$  is the effective diffusivity of chloride and is represented in terms of  $\times 10^{-12} \text{ m}^2/\text{s}$  in Eq. (12) and  $k_{Cl}$  is a fitting factor ranging from 103 to 297 for concrete [63,64]. The relative diffusivity predicted from the microstructures generated using CEMHYD3D for the experiments of Ma et al. [24] (electric-resistivity predictions) with the assumption that only nitrogen accessible C-S-H pores contribute to transport can be converted into a steady-state effective diffusivity of chloride ( $D_0$  for chloride taken as  $2.03 \times 10^{-9} \text{ m}^2/\text{s}$  [65]). Similarly, for the same dataset under the assumption that all C-S-H pores contributes to transport, the relative diffusivity can be converted into electric resistivity measurements (electric-resistivity of pore water  $\rho_0$ , taken as 0.21 Ohm-m, 0.25 Ohm-m and 0.29 Ohm-m for w/c equal to 0.3, 0.4 and 0.5, respectively [24]) Fig. 8 shows the relationship between electrical resistivity and the steady-state effective diffusivity of chlorides predicted from CEMHYD3D generated microstructure using the proposed C-S-H model. The fitted value of  $k_{Cl}$  for this dataset was obtained as 559.87 which is higher than the one reported for concrete. The lower values for concrete compared to cement paste can be attributed to dilution effect due to the presence of aggregates. For example, if the volume fraction of aggregates in concrete is 50% the corresponding value of  $k_{Cl}$  accounting for dilution effect would be around 279.5 ( $\approx (1 - 0.5) \times 559.87$ ).

### 3.3. General discussions

The above results clearly demonstrates that a better representation of depercolation of capillary pores (at around 20% capillary porosity), as is the case with CEMHYD3D microstructures, gives closer estimates to experimental results. One can argue that by lowering resolution of HMYOSTRUC microstructure artificial depercolation can be created. As shown in Fig. 9 for a 250  $\mu\text{m}$  length

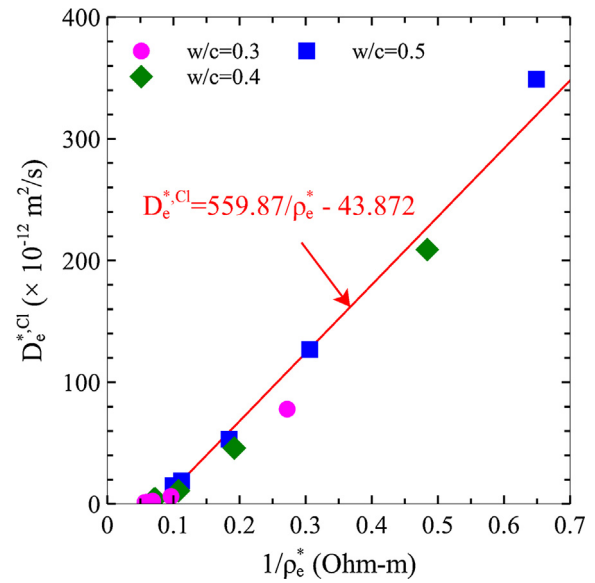


**Fig. 8.** Relationship between the steady-state chloride diffusion coefficient and effective resistivity obtained for cement composition of Ma et al. [24] from CEMHYD3D generated microstructure.

of REV cube, lowering resolution i.e. increasing grid spacing from 1  $\mu\text{m}$  to 5  $\mu\text{m}$ , reduces degree of percolation from 1 to circa 0.95. However it does not create depercolation of capillary porosity. For CEMHYD3D, Garboczi and Bentz [14] reported that percolation threshold is dependent on resolution. For a resolution of 0.25  $\mu\text{m}$  resolution the percolation threshold shifts to around 12% for capillary porosity. It should be noted that lowering of percolation threshold to 0.12 in CEMHYD3D generated microstructure, would result in higher diffusivity values for w/c between 0.4 and 0.5 due to the fact that a difference of up to two orders of magnitude can exist between diffusivity of C-S-H phase and capillary pores and therefore when capillary pores are connected capillary pores will be the most dominant diffusive phase. Thus, decreasing resolution does not result in depercolation in case of HYMOSTRUC and increasing resolution in case of CEMHYD3D would reduce percolation threshold, result in an overestimation of D.

As discussed previously, the shape of BBB affects the diffusivity values of C-S-H, and hence potentially influence the predicted diffusivity of cement paste. Fig. 10 shows the influence of the shape of the BBB of C-S-H on the diffusivity of cement paste predicted using CEMHYD3D generated microstructure for the experimental data of Béjaoui and Bary [48]. Considering the uncertainties in predictions and experimental data it can be concluded that the influence of the shape of BBB is negligible. Thus even though the C-S-H BBB do possess an aspect ratio from representation point of view in C-S-H diffusivity model aspect ratio is not a major factor.

Another important parameter in the above analysis is the constrictivity parameter for C-S-H phase. Fig. 11 shows the influence of constrictivity on diffusivity predicted using CEMHYD3D generated microstructure for the experimental data of Béjaoui and Bary [48]. The influence of constrictivity is proportional to the predicted diffusivity. For low w/c to mid w/c decrease in constrictivity would lead to decrease in diffusivity by same factor. This is due to the fact that for this microstructures, capillary pores are depercolated and C-S-H is the dominant diffusive phase. For high w/c ratios (0.6 and 0.65) the influence of the constrictivity parameter decreases as capillary pores are the dominant diffusive phase. However, a change of constrictivity still has a significant effect on predicted diffusivity. Fig. 11 shows that the choice of constrictivity parameter equal to 1/10 suggested by Bary and co-workers is reasonable

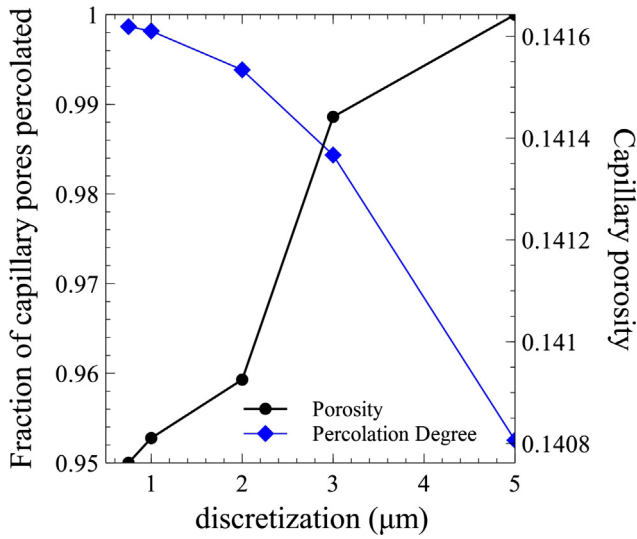


**Fig. 9.** Effect of microstructure resolution on percolation degree and porosity of HYMOSTRUC generated microstructures for w/c ratio of 0.45 (capillary porosity around 14%) for cement composition of Béjaoui and Bary [48]. Length of REV cube is 250 μm.

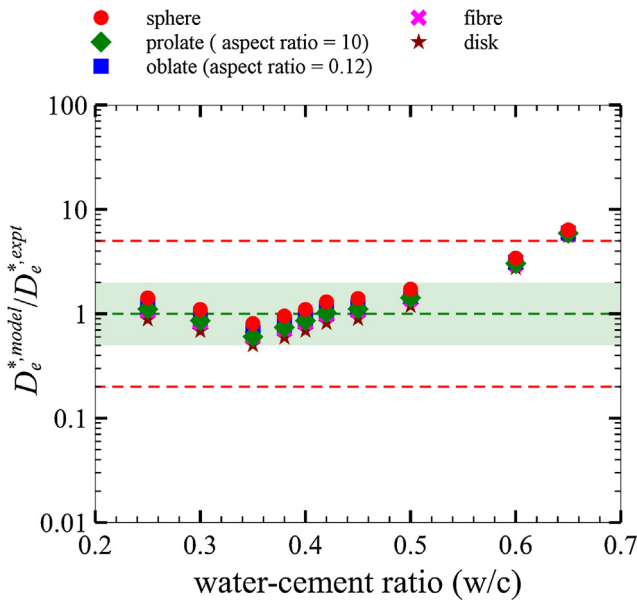


**Fig. 10.** ratio of effective diffusivity predicted from virtual microstructure ( $D_e^{*,model}$ ) corresponding to experimental data ( $D_e^{*,expt}$ ) with respect to w/c obtained using microstructures generated from CEMHYD3D for experimental data of [48] highlighting the influence of shape of BBB of C-S-H. Shaded green region shows factor 2-bounds and dashed line in red shows factor 5-bounds. (For interpretation of the references to colour in this figure caption, the reader is referred to the web version of this article.)

to achieve good predictions of diffusivity. More recently Phung et al. [66], experimentally determined that for ions with molecular diameter of 0.3–0.4 nm, which is the range for most of diffusing tracers used for experiments considered in this study, the constrictivity parameter is close to 1/10.

Finally, our simulations provide a viable postulate that for tracers such as HTO, dissolved helium and dissolved oxygen and ions, transport essentially occurs through nitrogen accessible gel pores, whereas all gel pores contribute to the electric resistivity measurements which explains the higher relative diffusivity measured by

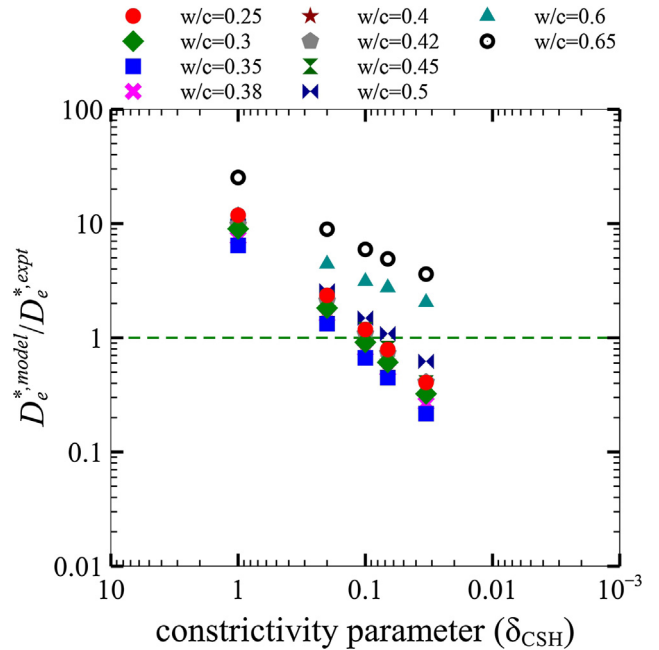


**Fig. 11.** Effect of constrictivity parameter on diffusivity predicted from virtual microstructure ( $D_e^{*,model}$ ) corresponding to experimental data ( $D_e^{*,expt}$ ) using microstructures generated from CEMHYD3D for experimental data of [48]. Shaded green region shows factor 2-bounds and dashed line in red shows factor 5-bounds. (For interpretation of the references to colour in this figure caption, the reader is referred to the web version of this article.)

the electric-resistivity experiments compared to the through-diffusion and electro-migration techniques. Jennings [67] suggested that the nitrogen accessible pores represent the large gel pores of sizes between 3–12 nm, whereas the nitrogen inaccessible pores represent small gel pores within range of 1–3 nm. The water in the small gel pores would be physically bound with different physical properties compared to the bulk pore water Jennings [67] and diffusion of tracers such as HTO, dissolved helium and dissolved oxygen seems to be difficult through this small gel pores. Moreover, due to negatively charged surface of of C-S-H their is higher concentration of calcium ions in the small gel pores [68]. The presence of calcium ions in these small pores can also retard movement of tracers [69]. On the other hand, due to excess concentration of calcium ions, zeta potential in the double layer is positive. Recently, in context of cement-based material, Nguyen et al. [70] through numerical simulation through nano cylindrical pores, accounting for positive zeta potential in double layer showed that for smaller pores conductivity will be higher compared to bulk water. This indicates that while diffusion of tracer in the small gel pores is negligible, the conductivity is still significant resulting in higher relative diffusivity measurements in resistivity experiments.

#### 4. Conclusions

Influence of capillary pore percolation and diffusion through gel pores on cement paste diffusivity has been explored using microstructures generated using HYMOSTRUC and CEMHYD3D. The goal of this study to utilize the fact that both models give different pore connectivity for same capillary pore fraction to investigate the role of capillary pore fraction. For diffusion through gel pores a continuum micro-mechanics based model for diffusivity has been proposed. Following conclusions can be drawn from the results in this study:

- The percolation threshold at around 20% for capillary porosity is essential in order to achieve good prediction of diffusivity for w/c ratios ranging from 0.3–0.5. In case of HYMOSTRUC capillary pores are fully percolated which results in over estimation of diffusivity at factor 10 at around 20% porosity. These differences diminish for the capillary porosity smaller or larger than percolation threshold. Further in case of electric resistivity, where the difference in C-S-H diffusivity and diffusivity of capillary pore phase is smaller, the effect of capillary pore depercolation is reduced. This in turn implies that the physical resolution for CEMHYD3D based microstructures should be restricted to 1  $\mu\text{m}$  to correctly represent depercolation and form HYMOSTRUC additional treatments are needed to achieve depercolation of large capillary pores. One way to achieve depercolation of capillary pores in HYMOSTRUC would be to consider that capillary pores can be divided in small capillary pores and large capillary pores with capillary pores smaller than 1  $\mu\text{m}$  present in LD C-S-H phase as suggested recently by Ma et al. [71].
- Differences up to an order of magnitude observed between electric-resistivity data and through-diffusion and electro-migration measurements at low w/c (low porosity) are due to differences in the diffusivity of C-S-H phase. From our analysis we postulate that for electric resistivity measurements all gel pores contribute to diffusivity, whereas, for through diffusion and electro-migration measurements diffusion occurs only through nitrogen accessible pores. The numerical approach presented here can be used to quantify the relationship between chloride diffusivity and electric resistivity which is of practical relevance.
- The choice of constrictivity parameter for C-S-H phase as 1/10 seems reasonable for chosen tracers. For low and mid range of w/c there is one to one correspondence between decrease in constrictivity and diffusivity. For high w/c (0.6 and 0.65) this is not the case but constrictivity parameter of C-S-H phase still has a significant effect on predicted diffusivity values.

Finally, the present study provides several postulates on mechanisms of diffusion in C-S-H pores and its effects on relative diffusivity. In future, detail studies at pore-scale considering electro-kinetics effects can provide further insights into differences in electrical resistivity measurements and diffusion of tracers. Similarly, molecular dynamics studies on mobility of tracers in small C-S-H pores can provide more physical understanding constrictivity parameter and restrictions of tracers to transport through small gel pores.

#### Appendix A. Two relaxation time Lattice Boltzmann method for mass transport

Lattice Boltzmann (LB) method solves the simplified form of discrete Boltzmann equation (discretized in space, time and velocity) which describes the evolution of a particle distribution function  $f_i(x, t)$ . Particle distribution function represents the probability of finding a particle with speed  $e_i$  at node  $x$  and time  $t$ . The governing equation to be recovered is then linked to LB equation through a multi-scale Chapman-Enskog expansion [72,73]. In this study a two relaxation time (TRT) variant of LB method [74] has been used. In two relaxation time (TRT) LB method the symmetric and anti-symmetric parts of the particle distribution function are relaxed separately using two different relaxation parameters. The symmetric ( $f^+$ ) and anti-symmetric parts ( $f^-$ ) of the particle distribution functions are defined as

$$f_i^+ = \frac{f_i + f_{-i}}{2} \quad \& \quad f_i^- = \frac{f_i - f_{-i}}{2} \quad (\text{A.1})$$

where  $f_i$  and  $f_{-i}$  refers to distribution functions corresponding to lattice speed  $e_i$  and  $e_{-i}$  respectively;  $e_i = -e_{-i}$ . The above definition of the symmetric and the anti-symmetric part naturally imposes a condition that all the even moments of the anti-symmetric part and odd moments of the symmetric parts are zero. The evolution of distribution function according to the TRT LB equation is given as follows [74]

$$f_i(x + e_i \Delta t, t + \Delta t) = f_i(x, t) + \Delta t \Omega_i^{\text{TRT}}(x, t) \quad (\text{A.2})$$

$$\Omega_i^{\text{TRT}}(x, t) = -\frac{1}{\tau_+} (f_i^+(x, t) - f_i^{\text{eq}+}(x, t)) - \frac{1}{\tau_-} (f_i^-(x, t) - f_i^{\text{eq}-}(x, t)) \quad (\text{A.3})$$

Here,  $\tau_+$  and  $\tau_-$  are relaxation parameters for the symmetric part and anti-symmetric part respectively. Additionally constraint is laid on the zero moment of  $f$  to ensure mass conservation.

$$\sum_i f_i = \sum_i f_i^{\text{eq}} = C \quad (\text{A.4})$$

In order to recover Eq. (1) from the Eq. (A.2) orthogonal lattices with 7 lattice direction (commonly referred to as D3Q7 lattice), along with the following equilibrium distribution function is sufficient

$$f_i^{\text{eq}} = \frac{C}{2} c_\phi \quad \forall i = 2, \dots, q \quad (\text{A.5})$$

$$f_1^{\text{eq}} = \phi C - \sum_{i>1} f_i \quad (\text{A.6})$$

where  $q$  being the number of lattice directions,  $c_\phi$  is the positive adjustable parameter. It can be shown through the multi-scale Chapman-Enskog analysis that the following equation Eq. (A.7) can be recovered from Eq. (A.2). The derivation follows a similar approach as the one in [75] in the case when velocity terms are neglected.

$$\frac{\partial \phi C}{\partial t} = \vec{\nabla} \cdot \left( \tau_- - \frac{\Delta t}{2} \right) \cdot \vec{\nabla} c_\phi C \quad (\text{A.7})$$

Comparing Eq. (A.7) with Eq. (1), the effective diffusion coefficient ( $D_e$ ) can be related to the relaxation parameter  $\tau_-$  as

$$D_e = c_\phi \left( \tau_- - \frac{\Delta t}{2} \right) \quad (\text{A.8})$$

In principle, both  $c_\phi$  and  $\tau_-$  can be varied in order to accommodate the spatial and temporal variations of the diffusion coefficient [75]. However, it can be seen from Eq. (A.7) that  $c_\phi$  should be spatially constant to remove it out of the gradient operator. Therefore, it is advisable to set  $c_\phi$  as constant throughout the domain to ensure correct recovery of Eq. (1). Moreover,  $c_\phi \leq \frac{\min(\phi)}{3}$  to ensure non-negativity of particle distribution function. In this study the  $c_\phi$  is taken as  $\frac{\min(\phi)}{3.5}$ . While  $\tau_-$  is related to the diffusion coefficient,  $\tau_+$  is the free parameter in TRT scheme, which can be adjusted to improve the stability or accuracy. The stability and accuracy of TRT scheme is related to the choice of the so called magic parameter ( $\Lambda$ ) which is defined as [76]

$$\Lambda = \left( \tau_- - \frac{1}{2} \right) \left( \tau_+ - \frac{1}{2} \right)$$

In our simulations the value  $\Lambda$  is fixed as 1/4 which ensures optimal stability for wide range of values of  $\tau_-$  and  $\tau_+$  [76]. LB simulations are usually carried out in LB units where in grid spacing and time step is set to one in LB units. The conversion between LB units and physical units is carried out through dimensional consideration as explained by the authors in [77]. In this study and  $\tau_-$  was set to one corresponding to  $D_0$  which was used to fix the time conversion factor and correspondingly  $\tau_-$  for other  $D_e$  values were obtained.

The initial concentration in the domain is set to zero and correspondingly the distribution function in all velocity directions is set to zero. To set boundary condition in LB schemes, the unknown

outgoing distribution function at end of each iteration has to be determined from the prescribed boundary condition in term of macroscopic variables. In case of D3Q7 lattice only one distribution function at boundary is unknown. Hence, to set the concentration boundary, unknown distribution function can be simply obtained as the difference between the concentration at the boundary and sum of incoming distribution function.

$$f_i = C_b - \sum_{j=1, j \neq i}^q f_j \quad (\text{A.9})$$

where  $C_b$  is the concentration at boundary [ $\text{NL}^{-3}$ ]. The zero flux boundary condition in LB method is implemented as a bounce back scheme, which essentially implies that the unknown incoming  $f_i$ 's at a given node are set to the outgoing  $f_i$ 's in opposite lattice direction.

$$f_i = f_{-i} \quad (\text{A.10})$$

The periodic boundary condition can be implemented in LB scheme by setting unknown distribution functions equal to the one at the opposite boundary i.e.,

$$\begin{aligned} f_i(x = 0, t + \Delta t) &= f_i(x = 100 \mu\text{m}, t) \\ f_i(x = 100 \mu\text{m}, t + \Delta t) &= f_i(x = 0, t) \end{aligned} \quad (\text{A.11})$$

As LB scheme is an explicit time marching scheme, iterations were stopped when the relative change in diffusivity obtained between two subsequent iterations is less than  $10^{-7}$ . This check was made every 50 iterations. In order to accelerate convergence to steady state PID based adaptive time-stepping scheme for LB methods developed by Patel [78] was used.

## Appendix B. Choice of effective media theory

Different continuum micro-mechanics based effective media theories exists for inclusion-matrix morphology, the most widely used being the Generalized Maxwell approximation (which is analogous to the Mori-Tanaka scheme used for elastic modulus [30]), the self-consistent scheme (and its variants, also referred to as effective media approximation [79]) and the differential effective media scheme. In the generalized Maxwell approximation, one phase is considered as inclusions in the other phase in an infinite domain with the same shape as the inclusion, so that a constant gradient can be assumed inside the domain. The inclusions are considered to be well separated so that they do not interact with each other. With this assumption, the analytical solution for a single inclusion can be directly applied to obtain the effective diffusivity of the composite with dilute concentrations of inclusions. In the self-consistent scheme, the phases are considered as inclusions in a matrix with a diffusivity equivalent to that of the effective diffusivity of the composite. It is further ensured that the local perturbations in a concentration field caused by these inclusions on average cancel out. The self-consistent scheme treats all phases of a heterogeneous medium in the same way and hence allows accounting for the effect of percolation of one phase into another phase. However, when the properties of different phases vary substantially, the self-consistent approximation fails [30] and spurious percolation thresholds are imposed. In the differential effective media scheme, one phase is taken as the matrix and another phase is added incrementally such that the added phase is always in the dilute limit with respect to current effective media. This assumption leads to a differential equation, integration of which gives the effective diffusivity of the composite. The differential effective media scheme ensures that the initial matrix is always connected. This in turn allows the differential effective media scheme to

recover Archie's relationship [80]. Furthermore, it has also been shown experimentally that the differential effective media theory can provide reasonable estimates for differently shaped inclusions at higher volume fractions [81]. It is known that even for low porosities cement paste matrix is diffusive. Therefore in order to avoid depercolation of pore in C-S-H volume element and to correctly account for higher volume fractions, in this study differential effective media theory was used to estimate effective diffusion coefficient

## Appendix C. Computation of $V_{\text{HD-CSH}}$ , $\phi_{\text{LD-CSH}}$ and $\phi_{\text{HD-CSH}}$

Capillary porosity ( $\phi_{\text{cp}}$ ) in cement paste is computed from the generated microstructures and gel porosity ( $\phi_{\text{gp}}$ ) is obtained by deducting capillary porosity from total porosity obtained using Power's model [51]

$$\phi_{\text{gp}} = \frac{w/c - 0.17\alpha}{w/c + 0.32} - \phi_{\text{cp}} \quad (\text{C.1})$$

The porosity of C-S-H volume element ( $\phi_{\text{CSH}}$ ) is then obtained by dividing gel porosity with C-S-H volume fraction ( $V_{\text{CSH}}$ ). Tennis and Jennings [37] provided an empirical formula for the ratio of mass of LD C-S-H to the mass of total C-S-H phase ( $M_r$ ) as

$$M_r = 3.017\alpha w/c - 1.347\alpha + 0.538 \quad (\text{C.2})$$

$\alpha$  is the degree of hydration and  $M_r$  is equivalent to the volume ratio of fraction of LD C-S-H solid ( $V_{\text{s,LD-CSH}}$ ) to solid in C-S-H ( $V_{\text{s,CSH}}$ ) as the solid phase density is same for both types of C-S-H. Solid in C-S-H is given as  $1 - \phi_{\text{CSH}}$ . As discussed previously, pores in C-S-H are divided into nitrogen accessible and inaccessible pores. Both LD and HD C-S-H contain the nitrogen inaccessible pores and the low density for LD C-S-H is due to additional nitrogen accessible pores. This implies density of HD C-S-H and LD C-S-H is same is nitrogen accessible pores are absent i.e.

$$\frac{M_{\text{HD-CSH}}}{V_{\text{s,HD-CSH}} + V_{\text{p,HD-CSH}}} = \frac{M_{\text{LD-CSH}}}{V_{\text{s,LD-CSH}} + V_{\text{p,LD-CSH}}^{\text{non-nit}}} \quad (\text{C.3})$$

where  $M_{\text{HD-CSH}}$  and  $M_{\text{LD-CSH}}$  represents mass of HD-CSH and LD-CSH respectively.  $V_{\text{p,HD-CSH}}$  and  $V_{\text{p,LD-CSH}}^{\text{non-nit}}$  denotes the fraction of HD pores and fraction of nitrogen inaccessible pores in LD C-S-H. As both LD C-S-H and HD C-S-H consist of same type of solids following relationship can be deduced between  $V_{\text{p,LD-CSH}}^{\text{non-nit}}$  and  $V_{\text{p,HD-CSH}}$

$$V_{\text{p,LD-CSH}}^{\text{non-nit}} = V_{\text{p,HD-CSH}} \frac{V_{\text{s,LD-CSH}}}{V_{\text{s,HD-CSH}}} \quad (\text{C.4})$$

$\phi_{\text{CSH}}$  can be thus represented as

$$\phi_{\text{CSH}} = \left( 1 + \frac{V_{\text{s,LD-CSH}}}{V_{\text{s,HD-CSH}}} \right) V_{\text{p,HD-CSH}} + V_{\text{nitro}} \quad (\text{C.5})$$

$V_{\text{nitro}}$  denotes the fraction nitrogen accessible pores in C-S-H and can be obtained using following relation [37]

$$V_{\text{nitro}} = \left( 1 - \frac{\rho_{\text{LD}}}{\rho_{\text{HD}}} \right) (V_{\text{s,LD-CSH}} + \phi_{\text{CSH}} - V_{\text{p,HD-CSH}}) \quad (\text{C.6})$$

$\rho_{\text{LD}}$  and  $\rho_{\text{HD}}$  are the dry densities of LD and HD C-S-H, respectively [ $\text{ML}^{-3}$ ]. The values of  $\rho_{\text{LD}}$  and  $\rho_{\text{HD}}$  are  $1.44 \text{ g/cm}^3$  and  $1.75 \text{ g/cm}^3$ , respectively [37]. Substituting Eq. (C.6) in Eq. (C.5) and rearranging  $V_{\text{p,HD-CSH}}$  can be obtained as

$$V_{\text{p,HD-CSH}} = \frac{(1 - Y)\phi_{\text{CSH}} - YV_{\text{s,LD-CSH}}}{X - Y} \quad (\text{C.7})$$

$$X = \left( 1 + \frac{V_{\text{s,LD-CSH}}}{V_{\text{s,HD-CSH}}} \right), Y = \left( 1 - \frac{\rho_{\text{LD}}}{\rho_{\text{HD}}} \right)$$

The volume fraction of HD C-S-H and the porosity of LD C-S-H and HD C-S-H can be determined as

$$V_{HD-C-S-H} = V_{p,HD-C-S-H} + V_{s,CSH} - V_{s,LD-C-S-H} \quad (C.8)$$

$$\phi_{LD-C-S-H} = \frac{V_{p,LD-C-S-H}^{non-nit} + V_{nitro}}{V_{p,LD-C-S-H}^{non-nit} + V_{nitro} + V_{s,LD-C-S-H}}$$

$$\phi_{HD-C-S-H} = \frac{V_{p,HD-C-S-H}}{V_{HD-C-S-H}}$$

## References

- [1] J.S. Dolado, K. Van Breugel, Recent advances in modeling for cementitious materials, *Cem. Concr. Res.* 41 (7) (2011) 711–726.
- [2] R.A. Patel, Q.T. Phung, S.C. Seetharam, J. Perko, D. Jacques, N. Maes, G.D. Schutter, G. Ye, K.V. Breugel, Diffusivity of saturated ordinary Portland cement-based materials: a critical review of experimental and analytical modelling approaches, *Cem. Concr. Res.* 90 (2016) 52–72.
- [3] D.P. Bentz, E. Garboczi, E. Lagergren, Multi-Scale Microstructural Modeling of Concrete Diffusivity: Identification of Significant Variables 20 (1) (1998) 129, ISSN 01496123, doi: <https://doi.org/10.1520/CCA10446J>, URL <http://www.astm.org/doiLink.cgi?CCAI0446J>.
- [4] J.J. Thomas, J.J. Biernacki, J.W. Bullard, S. Bishnoi, J.S. Dolado, G.W. Scherer, A. Lutttge, Modeling and simulation of cement hydration kinetics and microstructure development, *Cem. Concr. Res.* 41 (12) (2011) 1257–1278.
- [5] K.V. Breugel, Numerical simulation of hydration and microstructural development in hardening cement-based materials:(II) applications, *Cem. Concr. Res.* 25 (3) (1995) 522–530.
- [6] K.V. Breugel, Numerical simulation of hydration and microstructural development in hardening cement-based materials (I) theory, *Cem. Concr. Res.* 25 (2) (1995) 319–331.
- [7] G. Ye, K. Van Breugel, A. Fraaij, Three-dimensional microstructure analysis of numerically simulated cementitious materials, *Cem. Concr. Res.* 33 (2) (2003) 215–222.
- [8] N. Van Tuan, Rice husk ash as a mineral admixture for ultra high performance concrete (Ph.D. Thesis), TU Delft, 2011.
- [9] S. Bishnoi, K.L. Scrivener,  $\mu$ c: a new platform for modelling the hydration of cements, *Cem. Concr. Res.* 39 (4) (2009) 266–274.
- [10] D. Bentz, P. Coveney, E. Garboczi, M. Kleyn, P. Stutzman, Cellular automaton simulations of cement hydration and microstructure development, *Modell. Simul. Mater. Sci. Eng.* 2 (1994) 783.
- [11] D.P. Bentz, Three-dimensional computer simulation of portland cement hydration and microstructure development, *J. Am. Ceram. Soc.* 80 (1) (1997) 3–21. ISSN 00027820, DOI: <https://doi.org/10.1111/j.1151-2916.1997.tb02785.x>, URL <http://doi.wiley.com/10.1111/j.1151-2916.1997.tb02785.x>.
- [12] J.W. Bullard, E. Enjolras, W.L. George, S.G. Satterfield, J.E. Terrill, A parallel reaction-transport model applied to cement hydration and microstructure development, *Modell. Simul. Mater. Sci. Eng.* 18 (2) (2010) 025007.
- [13] G. Ye, Percolation of capillary pores in hardening cement pastes, *Cem. Concr. Res.* 35 (2005) 167–176.
- [14] E.J. Garboczi, D.P. Bentz, The effect of statistical fluctuation, finite size error, and digital resolution on the phase percolation and transport properties of the NIST cement hydration model, *Cem. Concr. Res.* 31 (10) (2001) 1501–1514.
- [15] D.P. Bentz, E.J. Garboczi, Percolation of phases in a three-dimensional cement paste microstructural model, *Cem. Concr. Res.* 21 (2–3) (1991) 325–344.
- [16] VCCTL software, <https://www.nist.gov/services-resources/software/vcctl-software> (online accessed on April 2016).
- [17] E.J. Garboczi, D.P. Bentz, Computer simulation of the diffusivity of cement-based materials, *J. Mater. Sci.* 27 (8) (1992) 2083–2092.
- [18] A. Atkinson, A.K. Nickerson, The diffusion of ions through water-saturated cement, *J. Mater. Sci.* 19 (9) (1984) 3068–3078.
- [19] C. Page, N. Short, A. El Tarras, Diffusion of chloride ions in hardened cement pastes, *Cem. Concr. Res.* 11 (3) (1981) 395–406.
- [20] D.P. Bentz, O.M. Jensen, A. Coats, F.P. Glasser, Influence of silica fume on diffusivity in cement-based materials: I. Experimental and computer modeling studies on cement pastes, *Cem. Concr. Res.* 30 (6) (2000) 953–962.
- [21] D. Bentz, E. Garboczi, H. Jennings, D. Quenard, Multi-scale digital-image-based modelling of cement-based materials, *MRS Online Proceedings Library Archive*, 370 (1994).
- [22] S. Kamali-Bernard, F. Bernard, W. Prince, Computer modelling of tritiated water diffusion test for cement based materials, *Comput. Mater. Sci.* 45 (2) (2009) 528–535.
- [23] A. Delagrave, J. Marchand, M. Pigeon, Influence of microstructure on the tritiated water diffusivity of mortars, *Adv. Cem. Based Mater.* 7 (97) (1998) 60–65, [https://doi.org/10.1016/S1065-7355\(97\)00029-1](https://doi.org/10.1016/S1065-7355(97)00029-1).
- [24] H. Ma, D. Hou, J. Liu, Z. Li, Estimate the relative electrical conductivity of  $Cn+5n+H$  gel from experimental results, *Constr. Build. Mater.* 71 (2014) 392–396, <https://doi.org/10.1016/j.conbuildmat.2014.08.036>.
- [25] B.H. Oh, S.Y. Jang, Prediction of diffusivity of concrete based on simple analytic equations, *Cem. Concr. Res.* 34 (2004) 463–480.
- [26] H. Ma, D. Hou, Z. Li, Two-scale modeling of transport properties of cement paste: Formation factor, electrical conductivity and chloride diffusivity, *Comput. Mater. Sci.* 110 (2015) 270–280.
- [27] M.Z. Zhang, G. Ye, K. Van Breugel, A numerical-statistical approach to determining the representative element volume (REV) of cement paste for measuring diffusivity, *Materiales de Construcción* 60 (300) (2010) 7–20.
- [28] N. Ukrainczyk, E.A.B. Koenders, Representative elementary volumes for 3D modeling of mass transport in cementitious materials, *Modell. Simul. Mater. Sci. Eng.* 22 (3) (2014) 035001.
- [29] K. Krabbenhoft, M. Hain, P. Wriggers, Computation of effective cement paste diffusivities from microtomographic images, in: *Composites with Micro- and Nano-Structure 2008*, pp. 281–297.
- [30] S. Torquato, *Random Heterogeneous Materials: Microstructure and Macroscopic Properties*, Springer Science & Business Media, ISBN 1475763557, 2013.
- [31] E. Stora, B. Bary, Q.C. He, On estimating the effective diffusive properties of hardened cement pastes, *Transp. Porous Media* 73 (3) (2008) 279–295.
- [32] B. Bary, S. Béjaoui, Assessment of diffusive and mechanical properties of hardened cement pastes using a multi-coated sphere assemblage model, *Cem. Concr. Res.* 36 (2) (2006) 245–258.
- [33] H.N. Bordallo, L.P. Aldridge, A. Desmedt, Water dynamics in hardened ordinary portland cement paste or concrete: from quasielastic neutron scattering, *J. Phys. Chem. B* 110 (36) (2006) 17966–17976.
- [34] H.M. Jennings, A model for the microstructure of calcium silicate hydrate in cement paste, *Cem. Concr. Res.* 30 (1) (2000) 101–116.
- [35] F. Ulm, G. Constantinides, Is concrete a poromechanics material? – A multiscale investigation of poroelastic properties, *Mater. Struct.* 37 (2004) 43–58.
- [36] H.M. Jennings, Refinements to colloid model of C-S-H in cement: CM-II, in: [67], 2008, pp. 275–289.
- [37] P.D. Tennis, H.M. Jennings, A model for two types of calcium silicate hydrate in the microstructure of Portland cement pastes, *Cem. Concr. Res.* 30 (6) (2000) 855–863.
- [38] G. Constantinides, F.J. Ulm, The effect of two types of C-S-H on the elasticity of cement-based materials: Results from nanoindentation and micromechanical modeling, *Cem. Concr. Res.* 34 (1) (2004) 67–80.
- [39] S. Garrault, E. Finot, E. Lesniewska, A. Nonat, Study of C-S-H growth on  $C_3S$  surface during its early hydration, *Mater. Struct.* 38 (4) (2005) 435–442.
- [40] W.-S. Chiang, E. Fratini, P. Baglioni, D. Liu, S.-H. Chen, Microstructure Determination of Calcium-Silicate-Hydrate Globules by Small-Angle Neutron Scattering, *The Journal of Physical Chemistry C* 116 (8) (2012) 5055–5061.
- [41] H.M. Jennings, B.J. Dalgleish, P.L. Pratt, Morphological development of hydrating tricalcium silicate as examined by electron microscopy techniques, *J. Am. Ceram. Soc.* 64 (10) (1981) 567–572.
- [42] J. Sanahuja, L. Dormieux, G. Chanvillard, Modelling elasticity of a hydrating cement paste, *Cem. Concr. Res.* 37 (10) (2007) 1427–1439.
- [43] H. Jennings, P. Tennis, Model for the developing microstructure in Portland cement pastes, *J. Am. Ceram. Soc.* 77 (12) (1994) 3161–3172.
- [44] N. Phan-Thien, D. Pham, Differential multiphase models for polydispersed spheroidal inclusions: thermal conductivity and effective viscosity, *Int. J. Eng. Sci.* 38 (1) (2000) 73–88.
- [45] V. Smilauer, Z. Bittnar, Microstructure-based micromechanical prediction of elastic properties in hydrating cement paste, *Cem. Concr. Res.* 36 (9) (2006) 1708–1718.
- [46] Q.T. Phung, Effects of Carbonation and Calcium Leaching on Microstructure and Transport Properties of Cement Pastes (Ph.D. Thesis), Ghent University, 2015.
- [47] T. Yamaguchi, K. Negishi, S. Hoshino, T. Tanaka, Modeling of diffusive mass transport in micropores in cement based materials, *Cem. Concr. Res.* 39 (12) (2009) 1149–1155.
- [48] S. Béjaoui, B. Bary, Modeling of the link between microstructure and effective diffusivity of cement pastes using a simplified composite model, *Cem. Concr. Res.* 37 (2007) 469–480.
- [49] V. Ngala, C. Page, Effects of Carbonation on Pore Structure and Diffusional Properties of Hydrated Cement Pastes, *Cem. Concr. Res.* 27 (7) (1997) 995–1007.
- [50] G.-W. Sun, W. Sun, Y.-S. Zhang, Z.-Y. Liu, Relationship between chloride diffusivity and pore structure of hardened cement paste, *Journal of Zhejiang University SCIENCE A* 12 (5) (2011) 360–367.
- [51] T.C. Hansen, Physical structure of hardened cement paste, *Mater. Struct.* 19 (6) (1986) 423–436.
- [52] B.J. Christensen, T.O. Mason, H.M. Jennings, D.P. Bentz, E.J. Garboczi, Experimental and computer simulation results for the electrical conductivity of portland cement paste, *Materials Research Society Symposium Proceeding* 245 (1992) 259–264.
- [53] G.G. Taffinder, B. Batchelor, Measurement of Effective Diffusivities in Solidified Wastes, *J. Environ. Eng.* 119 (1) (1993) 17–33. ISSN 0733–9372.
- [54] P. Tumidajski, A.S. Schumacher, S. Perron, P. Gu, J. Beaudoin, On The Relationship Between Porosity and Electrical Resistivity in Cementitious Systems, *Cem. Concr. Res.* 26 (4) (1996) 539–544.
- [55] K. Van Breugel, Simulation of hydration and formation of structure in hardening cement-based materials, Ph.D. dissertation, TU Delft, Delft, 1991.
- [56] L. Liu, W. Sun, G. Ye, H. Chen, Z. Qian, Estimation of the ionic diffusivity of virtual cement paste by random walk algorithm, *Constr. Build. Mater.* 28 (1) (2012) 405–413.

- [57] M. Zhang, G. Ye, K. Van Breugel, Microstructure-based modeling of water diffusivity in cement paste, *Constr. Build. Mater.* 25 (4) (2011) 2046–2052.
- [58] G. Sant, D. Bentz, J. Weiss, Capillary porosity depercolation in cement-based materials: Measurement techniques and factors which influence their interpretation, *Cem. Concr. Res.* 41 (8) (2011) 854–864.
- [59] W. McCarter, T. Chrisp, G. Starrs, A. Adamson, E. Owens, P. Basheer, S. Nanukuttan, S. Srinivasan, N. Holmes, Developments in performance monitoring of concrete exposed to extreme environments, *Journal of Infrastructure Systems* 18 (3) (2011) 167–175.
- [60] P. Basheer, P. Gilleece, A. Long, W. Mc Carter, Monitoring electrical resistance of concretes containing alternative cementitious materials to assess their resistance to chloride penetration, *Cement and Concrete Composites* 24 (5) (2002) 437–449.
- [61] M. Torres-Luque, E. Bastidas-Arteaga, F. Schoefs, M. Sánchez-Silva, J. Osma, Non-destructive methods for measuring chloride ingress into concrete: State-of-the-art and future challenges, *Constr. Build. Mater.* 68 (2014) 68–81. ISSN 0950-0618.
- [62] C. Andrade, R. Andrea, Electrical resistivity as microstructural parameter for modelling of service life of reinforced concrete structures, in: K. van Breugel, G. Ye, Y. Yuan (Eds.), 2nd International Symposium on Service Life Design for Infrastructure, Delft, Netherlands, 2010, pp. 379–388.
- [63] L. Tang, L.-O. Nilsson, P.M. Basheer, Resistance of Concrete to Chloride Ingress: Testing and Modelling, CRC Press, 2011.
- [64] V. Baroghel-Bouny, K. Kinomura, M. Thiery, S. Moscardelli, Easy assessment of durability indicators for service life prediction or quality control of concretes with high volumes of supplementary cementitious materials, *Cem. Concr. Compos.* 33 (8) (2011) 832–847.
- [65] V. Ngala, C. Page, L. Parrott, S. Yu, Diffusion in cementitious materials: II, further investigations of chloride and oxygen diffusion in well-cured OPC and OPC/30%PFA pastes, *Cem. Concr. Res.* 25 (4) (1995) 819–826.
- [66] Q.T. Phung, N. Maes, E. Jacobs, D. Jacques, G. De Schutter, G. Ye, Insights and issues on the correlation between diffusion and microstructure of saturated cement pastes, *Cem. Concr. Res.*, CEMCON\_2017\_447 (under review).
- [67] H.M. Jennings, Refinements to colloid model of C-S-H in cement: CM-II, *Cem. Concr. Res.* 38 (3) (2008) 275–289.
- [68] R.-M. Pellenq, N. Lequeux, H. van Damme, Engineering the bonding scheme in C-S-H: the ionic-covalent framework, *Cem. Concr. Res.* 38 (2) (2008) 159–174, <https://doi.org/10.1016/j.cemconres.2007.09.026>. ISSN 0008-8846, URL <http://www.sciencedirect.com/science/article/pii/S0008884607002372>, special Issue – The 12th International Congress on the Chemistry of Cement. Montreal, Canada, July 8–13.
- [69] Y. Zhou, D. Hou, J. Jiang, W. She, J. Li, Molecular dynamics study on the solvated aniline (AN) and ethylene glycol (EG) monomers confined in calcium silicate nanometer channel: a case study of Tobermorite, *Phys. Chem. Chem. Phys.* (2017).
- [70] Q.H. Nguyen, S. Lorente, A. Duhard-Barone, Effect of the pore size of cement based materials on ionic transport, *Constr. Build. Mater.* 147 (Supplement C) (2017) 160–167. ISSN 0950-0618.
- [71] H. Ma, D. Hou, Y. Lu, Z. Li, Two-scale modeling of the capillary network in hydrated cement paste, *Constr. Build. Mater.* 64 (2014) 11–21.
- [72] S. Succi, *The Lattice Boltzmann Equation: for Fluid dynamics and Beyond*, Oxford University Press, 2001.
- [73] D.A. Wolf-Gladrow, *Lattice-gas Cellular Automata and Lattice Boltzmann Models: An Introduction*, Springer Science & Business Media, 2000.
- [74] I. Ginzburg, Equilibrium-type and link-type lattice Boltzmann models for generic advection and anisotropic-dispersion equation, *Adv. Water Resour.* 28 (11) (2005) 1171–1195.
- [75] A. Vikhansky, I. Ginzburg, Taylor dispersion in heterogeneous porous media: extended method of moments, theory, and modelling with two-relaxation-times lattice Boltzmann scheme, *Phys. Fluids* 26 (2) (2014) 022104.
- [76] I. Ginzburg, D. D'Humières, A. Kuzmin, Optimal stability of advection-diffusion lattice Boltzmann models with two relaxation times for positive/negative equilibrium, *J. Stat. Phys.* 139 (6) (2010) 1090–1143.
- [77] R.A. Patel, J. Perko, D. Jacques, G. De Schutter, K. Van Breugel, G. Ye, A versatile pore-scale multicomponent reactive transport approach based on lattice Boltzmann method: Application to portlandite dissolution, *Phys. Chem. Earth.* (2014) 70–71. ISSN 14747065.
- [78] R.A. Patel, Lattice Boltzmann Method Based Framework for Simulating Physico-chemical Processes in Heterogenous Porous Media and its Application to Cement Paste (Ph.D. Thesis), Ghent University, 2016.
- [79] A. Norris, A differential scheme for the effective moduli of composites, *Mech. Mater.* 4 (1) (1985) 1–16.
- [80] P.N. Sen, C. Scala, M.H. Cohen, A self-similar model for sedimentary rocks with application to the dielectric constant of fused glass beads, *Geophysics* 46 (5) (1981) 781–795.
- [81] L. Weber, J. Dorn, A. Mortensen, On the electrical conductivity of metal matrix composites containing high volume fractions of non-conducting inclusions, *Acta Mater.* 51 (11) (2003) 3199–3211.